Swelling and Dissolution Kinetics of Natural and Man-Made Cellulose Fibers in Solvent Power Tuned Ionic Liquid

Feng Chen [a], Daisuke Sawada [a], Michael Hummel [a], Herbert Sixta [a], Tatiana Budtova [a, b, *]

[a] *Department of Bioproducts and Biosystems, School of Chemical Engineering, Aalto University, P.O. Box 16300, 00076 Aalto, Helsinki, Finland;*

[b] *MINES ParisTech, PSL Research University, Center for Materials Forming-CEMEF, UMR CNRS 7635, CS 10207, 06904 Sophia Antipolis, France.*

* Correspondence: tatiana.budtova@mines-paristech.fr, tatiana.budtova@aalto.fi

Abstract: The kinetics of the dissolution and swelling of different cellulose fibers in the ionic liquid 1-ethyl-3-methylimidazolium acetate ([EMIM][OAc]) was studied by varying solvent power and temperature. Natural fiber, flax, and man-made fibers, Cordenka and Lyocell-type (Ioncell) were used with one Ioncell fiber containing lignin and hemicelluloses. Through the addition of water, the solvent power was modified from very good (neat ionic liquid), to moderate (with 5 wt.% water) and weak (15 wt.% water). The temperature was varied to correlate the fiber dissolution rate with the solvent viscosity. All fibers were characterized by chemical composition, crystallinity, molecular weight distribution and dynamic vapor sorption. It was demonstrated that while the rate of fiber dissolution in neat ionic liquid depends on fiber accessibility and solvent viscosity, the water-induced decreased solvent power dominates the general fiber behavior. Flax appeared to be the most "sensitive" to the solvent power due to its hierarchical structure. The fastest dissolution or swelling was recorded for Ioncell and the slowest for Cordenka.

Keywords: *cellulose fiber, ionic liquid, dissolution, swelling, accessibility*

1 Introduction

Cellulose is a fascinating biopolymer present on the Earth in almost inexhaustible quantity. It is a linear polymer built of anhydroglucose units linked by (1→4)-β glycosidic bonds, and until recently it was used mainly for making paper, textile fibers and films (Klemm et al. 2005; Ragauskas et al. 2006). Cellulose cannot be melt-processed (Chen et al. 2015) and thus its shaping requires dissolution (Gross et al. 2010). During the past decades, new cellulose-based materials were developed involving complete or partial dissolution, for example, aerogels (Budtova 2019) and all-cellulose composites (Takashi et al. 2004).

Several direct cellulose solvents are known, with LiCl/N,N-dimethylacetamide (DMAc) (McCormick et al. 1985), NaOH-based aqueous solutions (Budtova and Navard 2016), N-methylmorpholine N-oxide (NMMO) monohydrate (Fink et al. 2001) and ionic liquids (ILs) (Swatloski et al. 2002) being the most popular ones. Among these solvents, only NMMO monohydrate is used as direct cellulose solvent on an industrial scale for spinning textile fibers (Lyocell process); the use of ionic liquids, resulting in Ioncell fibers (also Lyocell process), is seen as approach alternative to that using NMMO-based technology (Sixta et al. 2015).

While fibers, films and aerogels require complete cellulose dissolution, all-cellulose composites are based on partial dissolution of natural or man-made fibers (Takashi et al. 2004; Soykeabkaew et al. 2009; Huber et al. 2012). All-cellulose composites are produced either by the dissolution of the surface of cellulose fibers with the dissolved cellulose "gluing" fibers together upon coagulation (Huber et al. 2012), or by dispersing cellulose fibers in a cellulose solution, the latter acting as a continuous matrix (Korhonen et al. 2019). To control the properties of all-cellulose composite, the understanding and quantification of the kinetics of fiber dissolution is a prerequisite. Too short dissolution times will result in an insufficient amount of dissolved cellulose in-between the fibers while too long dissolution will result in the destruction of natural fibers' cell walls and the formation of excessive amount of mechanically weaker cellulose II.

Although the dissolution of cellulose fibers in various direct solvents has been studied since the first half of the 20th century, detailed investigations of the dissolution mechanisms emerged only during the past 20 years due to a significant improvement of analytical tools. For example, the development of optical microscopy with various set-ups allowed for precise visualization, temperature control, video capture, and image analysis to follow the fibers' evolution during dissolution. The majority of studies was focusing on wood fibers (Olsson

et al. 2014; Cuissinat et al. 2006; Mäkelä et al. 2018; Le Moigne et al. 2010; Parviainen et al. 2014), most probably because of practical reasons, as films and textile fibers are made from wood dissolving pulps. By varying the solvent dissolution power, it was demonstrated that wood fibers dissolve either directly from the surface resulting in their diameter decrease, sometimes by disintegration into particles, or via ballooning followed by their burst (Cuissinat et al. 2006). In moderate and bad solvents fibers only swell either via ballooning or by a homogeneous increase in diameter, respectively (Cuissinat et al. 2006). The same mechanisms apply to cotton fibers but, interestingly, not to flax or ramie (Cuissinat et al. 2008). Lyocell fibers either radially dissolve in a good solvent or radially swell in a moderate solvent (Chaudemanche et al. 2011). Various factors have to be taken into account to understand fiber swelling and dissolution behavior: their composition, properties of primary and secondary layers in natural fibers or properties of a skin in man-made fibers (Abu-Rous et al. 2007), accessibility, porosity, and ,potentially, cellulose crystallinity and molecular weight.

The studies of the kinetics of fiber dissolution are very scarce. Microcrystalline cellulose was used as a model substance to study the kinetics of its dissolution in ionic liquids and the influence of a co-solvent, dimethylsulfoxide (DMSO), on the dissolution (Andanson et al. 2014). Cellulose dissolution was assessed by the decrease of birefringence which arises from the crystalline regions in polarized light (Andanson et al. 2014). Optical microscopy coupled with semi-automated data processing was used to evaluate the dissolution kinetics of two kraft pulps in 0.2 M cupriethylene diamine by tracing the fiber surface area (Mäkelä et al. 2018). A first-order kinetic model was shown to be applicable to describe fibers' dissolution (Mäkelä et al. 2018). The kinetics of wood fiber homogeneous swelling in NMMO in the presence of water at 18–22 % was reported by H. Peng et al. (Peng et al. 2017). To the best of our knowledge, there is no report comparing the kinetics of dissolution and/or swelling of different fibers, natural and man-made, under the same conditions. In the view of making all-cellulose composites, the evolution of long natural fibers, such as flax, are of particular interest (Chen et al. 2020). The beginning of the dissolution and/or swelling processes is of special importance and has to be well understood and controlled.

The goal of this work was to perform a comprehensive study comparing both the dissolution and swelling kinetics of flax and various man-made fibers with different characteristics. Room temperature ionic liquid, 1-ethyl-3-methylimidazolium acetate ([EMIM][OAc]), was used, and temperature was varied to tune solvent viscosity. Solvent dissolution power was varied by adding water. The correlations between fiber dissolution

and swelling kinetics, fiber characteristics (structure, composition, cellulose molecular weight and accessibility), solvent power and viscosity were built.

2 Experimental Part

2.1 Materials

Flax fibers were from the outer bast layer of the plant stem. A commercially available high-strength rayon filament yarn Cordenka 700 was kindly donated by Cordenka GmbH & Co. KG., and two other man-made fibers were produced by spinning of an unbleached birch kraft pulp-ionic liquid solutions resulting in Ioncell-FL fibers (coded "H50" in the ref. Ma et al. 2018), and of a prehydrolysed kraft birch pulp-IL solution, resulting in Ioncell-F fibers (see, for example, Asadi et al. 2018). The characteristics of the fibers are presented in the Results section. The ionic liquid 1-ethyl-3-methylimidazolium acetate ([EMIM][OAc]), purity > 95%, was purchased from IoLiTec, Germany. The moisture content of [EMIM][OAc] was 0.27 wt.% as determined by Karl-Fischer titration. The milli-Q® water was used to dilute the IL to IL-water mixtures to tune solvent power.

2.2 Methods

2.2.1 Chemical composition of fibers

The composition (carbohydrates, total lignin) of all fibers was determined according to NREL/TP-510-42618 norm. The amount of carbohydrates was detected by high performance anion exchange chromatography with pulse amperometric detection (HPAEC-PAD) using a Dionex ICS-300 system. Cellulose and hemicellulose contents were calculated according to the amount of monosaccharides following the Janson formula (Janson 1970). The acid-soluble lignin was determined by using a Shimadzu UV 2550 spectrophotometer at a wavelength of 205 nm using absorption coefficient of 110 $Lg^{-1}cm^{-1}$.

2.2.2 Molecular weight distribution of cellulose in fibers

The molecular weight distribution of cellulose in all fibers was characterized by gel permeation chromatography (GPC) according to the procedure described elsewhere (Ma et al. 2018), and number-average and weight-average molecular weights, M_n and M_w, were calculated. Prior to the analysis, fibers were cut into small pieces. The GPC system consisted of a pre-column (PLgel Mixed-A, 7.5 × 50 mm), four analytical columns (4 × PLgel Mixed-

A, 7.5 × 300 mm) and a RI-detector (Shodex RI-101). The fibers were pre-activated by water/acetone/DMAc solvent exchange sequence. The samples were then dissolved in a 90 g/L lithium chloride (LiCl)/DMAc mixture at room temperature. The solution was diluted to 9 g/L LiCl/DMAc, filtered through a 0.2 mm syringe filter and analyzed by using a Dionex Ultimate 3000 system with refractive index (RI) detection (Shodex RI-101).

2.2.3 Determination of the crystallinity index by X-ray diffractometer (XRD)

XRD patterns were collected on an X-ray diffractometer (a X'Pert Pro MRD, PAN'alytical, Lelyweg, The Netherlands) with Cu-Kα radiation (λ = 1.5418 Å). Fiber samples were grinded to powder and then mounted on multi-position sample holder. Data were collected in a 2θ range between 5° and 60° in reflection mode.

The background profile was estimated using a smoothing method (Brückner 2000; Frost et al. 2009) applying Savitzky-Golay (Savitzky et al. 1964) filter in the 2θ range from 6 to 55° for each diffraction profile. Window size and polynomial order for the Savitzky-Golay filter were set to 51 data points (corresponding to 4° by 2θ) and 1, respectively. Iteration for the background estimation was repeated 50 times. The crystallinity index (CRI_{total}) of fibers was estimated using the ratio of the area of total intensity (I_{total}) and of background intensity (I_{bkg}) from 10 to 30° 2θ:

$$CRI_{total} = 100 \times \frac{\int I_{total}\, d2\theta - \int I_{bkg}\, d2\theta}{\int I_{total}\, d2\theta} \quad (1)$$

In this method the crystallinity index is calculated over the total material.

2.2.4 Dynamic vapor sorption (DVS)

A dynamic vapor sorption apparatus with a measuring accuracy of 0.1 mg was used to record kinetics of water vapor sorption by the fibers. Around 15 mg of grinded fibers were placed in the sample pan and their weight evolution was recorded upon decrease of the relative humidity (RH) to 0 % at 25 °C under nitrogen (flow rate 100 cm^3/s). Equilibrium was considered to be reached when sample mass change was below 0.001 % per minute over 10 min. Then RH was increased to 60 % and sample weight evolution and time to reach equilibrium (t_s) were recorded. Moisture desorption M_{des} (from M_{amb} at ambient conditions to M_0 at 0% RH) and sorption M_s (from M_0 to M_{60} at 60% RH) were calculated as follows:

$$M_{des} = \frac{M_{amb} - M_0}{M_0} \times 100\% \quad (2)$$

$$M_s = \frac{M_{60} - M_0}{M_0} \times 100\% \quad (3)$$

2.2.5 Rheological characterization

The rheological properties of the IL and IL-water mixtures were characterized using an Anton Paar MCR 302 rheometer equipped with a plate-plate geometry (25 mm plate diameter, 1 mm gap) and a Peltier temperature control system. Viscosity-shear rate dependences were recorded from 1 to 100 s^{-1} at fixed temperature which was varied from 20 °C to 60 °C.

2.2.6 Kamlet−Taft Parameters

The Kamlet−Taft parameters of the neat [EMIM][OAc] and [EMIM][OAc]-water mixtures were determined from the absorption peaks of three different dyes: Reichardt's dye (RD, range 518−585 nm), *N*,*N*-diethyl-4-nitroaniline (DENA, 402−414 nm), and 4-nitroaniline (NA, 406−398 nm). The dyes were weighed and mixed with the IL or IL-water mixture. A Varian UV−vis spectrometer equipped with a thermostat (precision ± 0.1 °C) was used. The milli-Q® water was measured for background subtraction. Spectra were collected at a resolution of 1 nm and 10−30 nm of absorbance and data around the peak were fitted with a Gaussian function in order to precisely locate the maximum (ν_{max}). More details on the measurement of Kamlet-Taft parameters can be found in Hauru et al. 2012.

2.2.7 Optical microscopy observations of fiber swelling and dissolution

One fiber was placed between two glass plates with the in-between distance around 140 μm controlled by spacers. The distance between two glass slides is much larger than the fiber's thickness. As the proportion between fiber and solvent was approximately 7×10^{-4} g/g, we assume that the fiber was in an infinite solvent, i.e. the overall polymer concentration during and after complete dissolution can be neglected. The ends of the fiber were fixed by tape and solvent added. Fiber diameter was recorded by a DM4500P (Leica) optical microscope in transmission mode equipped with a CCD camera (Metallux 3, Leitz) and Linkam TMS 91 hot stage to control temperature. The evolution of the fiber diameter in time t was calculated as D_t/D_0, where D_0 and D_t are initial diameter of the fiber at t = 0 and diameter of fiber at time t, respectively.

3 Results

This section is structured as follows. Because different types of fibers were studied, their composition, cellulose molecular weight, crystallinity index and accessibility are reported first. Then solvent properties, such as Kamlet-Taft parameters and viscosity as a function of temperature and water content, are presented. Based on these results, solvents to study fiber swelling and dissolution were selected. Finally, the fiber behavior upon the addition of the solvents at different temperatures, monitored with optical microscopy, are presented and discussed.

3.1 Physiochemical properties of cellulose fibers

Flax is a natural fiber with a complex morphology; its elementary fiber consists of several cell wall layers and a lumen. The outer layer (or a primary cell wall) is the first layer formed during the cell wall growth; it is relatively thin and contains mainly less ordered cellulose, hemicelluloses and pectins. The secondary cell wall is much thicker than the primary wall and consists of highly crystalline cellulose fibrils spirally wound in a matrix of hemicellulose and pectins. Cellulose fibrils in this layer are oriented in the axis of the fiber and hence display a unidirectional structure (Rong et al. 2001; Charlet et al. 2010; Baley 2002). Two types of man-made fibers were selected, Cordenka, a modified viscose fiber, and Lyocell-type Ioncell fibers. Cordenka consists of a dense skin and spongy core (Rous et al. 2006). Fibers made via Lyocell process have more homogeneous morphology, with a semipermeable skin, porous middle zone and dense fiber center (Rous et al. 2006; Rous et al. 2007).

The composition of the fibers used in this work is shown in Table 1. Flax contains 83.3% cellulose, 11.3% hemicellulose and 2.3% lignin; the results are in line with those reported in literature (Yan et al. 2014; Bolton 1994). Cordenka filament is spun from a high-grade dissolving pulp and thus contains only small amounts of hemicellulose. Ioncell-F, prepared from a standard dissolving-grade pulp, has a higher hemicellulose content. Ioncell-FL is spun from an unbleached kraft pulp and thus contains notable amounts of both hemicellulose and lignin.

Table 1. Characteristics of fibers used in this study

Samples	Cellulose %	Hemicellulose %	Lignin %	M_n kDa	M_w kDa	CRI_{total} %	M_{des} %	M_s %	t_s min
Flax	83.3	11.3	2.3	652	714	45.1	1.3	7.15	115.7
Cordenka	92.3	2.4	-	68	133	28.1	7.2	11.91	305.2
Ioncell-F	88.9	8.2	-	45	134	40.3	7.5	9.82	177.5
Ioncell-FL	51.1	21.3	22.9	45	176	27.3	10	9.87	177.5

The number-average (M_n) and weight-average (M_w) molecular weights of cellulose in each fiber are presented in Table 1, and the corresponding molecular weight distributions are shown in Figure 1a. The results are similar for all man-made fibers and are much higher for flax. A distinct low molecular weight peak for Ioncell-FL and a subtle shoulder for flax and Ioncell-F correspond to the hemicellulose fraction, as shown in Table 1.

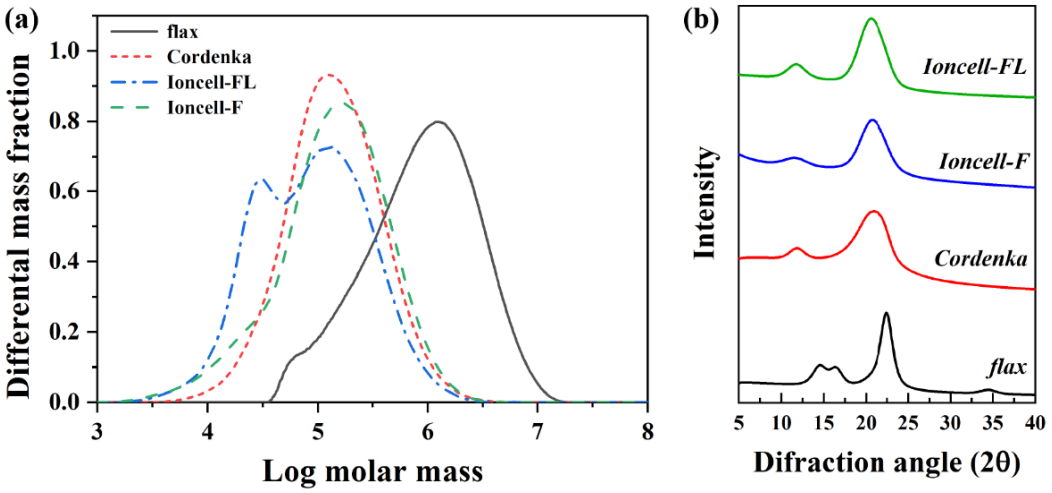

Fig. 1 Cellulose molecular mass distribution (a) and X-ray diffraction profiles (b) of flax, Cordenka, Ioncell-F and Ioncell-FL

Figure 1b presents the XRD profiles of all fibers. Flax contains cellulose I with crystallinity index of around 45%, which is typical for plant cellulose (Placet et al. 2012;

Moryganov et al. 2018). The man-made fibers contain the cellulose II allomorph, as expected. The crystallinity index (CRI_{total}) is around 28 %, 40 % and 27 % for Cordenka, Ioncell-F and Ioncell-FL, respectively (Table 1). Cordenka, a viscose type cellulose fiber, has low crystallinity, in-line with data in literature (Kreze et al. 2003; Okubayashi et al. 2005). As the crystallinity is calculated over the total material, and non-cellulose fraction in Ioncell-FL is around 50%, cellulose crystallinity in Ioncell-FL is higher than CRI_{total}; for this fiber it was reported to be around 40% (Ma et al. 2018).

To compare the accessibility of the fibers, the dynamic water vapor desorption and sorption were measured. The desorption (to 0% RH) and sorption (to 60% RH) curves are shown in Figure S1. Moisture desorption (M_{des}), time to reach equilibrium t_s from 0 to 60 %RH and moisture sorption (M_s) for each fiber are shown in Table 1 (see also Methods sections and eqs. 2 and 3). M_{des} reflects the amount of water which is desorbed from ambient conditions to 0 % RH and it is the lowest for flax. Cordenka, as viscose fiber, absorbs the highest amount of moisture (M_s) due to its lowest crystallinity and larger pore volume (Okubayashi et al. 2005). Time to reach equilibrium, t_s = 305.2 s, is the longest for Cordenka (Table 1) probably because of hornification phenomena (Siroka et al. 2008) as viscose fibers can be overdried, and also because absorption of a larger amount of vapor takes more time. The lignin-free fiber Ioncell-F and lignin-containing fiber Ioncell-FL show the same moisture sorption characteristics, similar to those of commercial Lyocell fibers with a moisture sorption around 9% - 10% at 60% RH and room temperature (Okubayashi et al. 2004). The presence of hydrophobic lignin does not influence the water vapor sorption behavior, in line with previously reported results (Ma et al. 2015). Flax absorbs the least amount of vapor probably because of the "resistant" primary wall (Okubayashi et al. 2004; Xie et al. 2011; Le Moigne et al. 2008) and higher cellulose crystallinity (Table 1).

3.2 [EMIM][OAc] and [EMIM][OAc]-water properties

It was demonstrated that the dissolution power of cellulose solvents is correlated with the Kamlet−Taft parameters β (H-bond basicity) and α (H-bond acidity) (Spange et al. 1998; Fukaya et al. 2006). β describes the ability to accept hydrogen bonds and has been correlated to the breakage of inter- and intra-chain hydrogen bonds within the cellulose chains. High β values were found to positively correlate with cellulose dissolution. In solvent systems with more than one component, as aqueous solutions of ionic liquids, each species might act predominantly as hydrogen bond acceptor or donor. The anions in cellulose-dissolving ILs

usually accept H-bonds, and thus are mostly responsible for the total β value. However, in mixtures of ionic liquid and water, water competes with the hydroxyl groups of cellulose for the hydrogen bond acceptance of the anion. It was demonstrated that the ability of such solvents to dissolve cellulose is described by β−α (net basicity) which takes the adverse effect of any intrinsic H-donor into account (Hauru et al. 2012). It was further shown that cellulose solvents should be located in a region roughly defined by $0.80 < \beta < 1.20$ and $0.35 < \beta-\alpha < 0.9$ with higher dissolution power corresponding to higher values within these intervals (Hauru et al. 2012). The Kamlet−Taft parameters of [EMIM][OAc] with different water contents were measured in the range of 20 - 60 ℃. Figure 2 shows the values of β and β-α as a function of water content at 25 ℃ and 60 ℃; the effect of temperature on Kamlet-Taft values was very small. Within the range of the studied water content, both β and β-α values show a linear decrease with the increase of water content indicating a decreased dissolution ability with 15 wt.% water being at the limit of the solubility window. It was reported that above 15 wt.% water in [EMIM][OAc] microcrystalline cellulose is not dissolved but forms swollen aggregates (Le et al. 2012). Therefore, in the following study [EMIM][OAc] containing 0, 5 and 15 wt.% of water was used as solvents with different power to monitor fiber swelling and dissolution behavior.

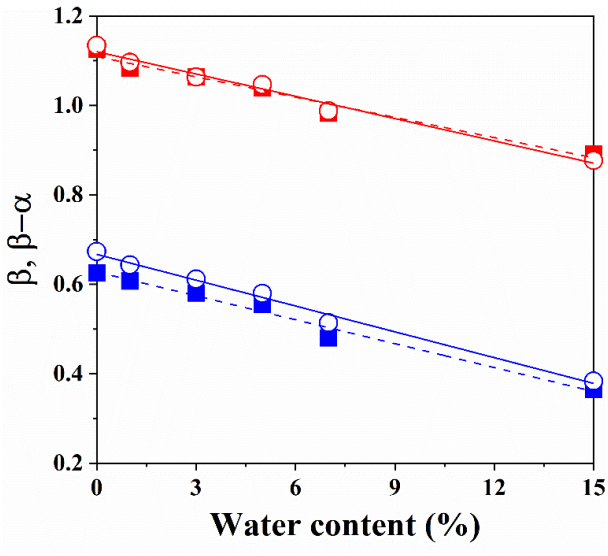

Fig. 2 β (red symbols) and β−α (blue symbols) plotted against water content in IL [EMIM][OAc] at 25 ℃ (solid symbol) and 60 ℃ (open symbol)

Solvent viscosity is another important parameter to consider for polymer dissolution. In general, for the same solvent quality and at the same temperature, lower viscosity should accelerate the dissolution rate because of a quicker solvent diffusion. On the one hand, the

addition of water to [EMIM][OAc] is known to decrease ionic liquid viscosity (Hall et al. 2012), but on the other hand, water is cellulose anti-solvent. In order to take both solvent characteristics into account, we measured the viscosity of [EMIM][OAc] with various water content of 0 – 15 wt.% as a function of shear rate at different temperatures (Figure S2). All studied mixtures are Newtonian liquids. Their viscosity is plotted as a function of water content at 25, 30 and 40 °C; the arrows show that [EMIM][OAc] at 40 °C and [EMIM][OAc]-5 wt.% water at 30 °C have the same viscosity (Figure 3). These two solvents will be used in the following as an example of a solvent with the same viscosity but different dissolution power (Figure 2).

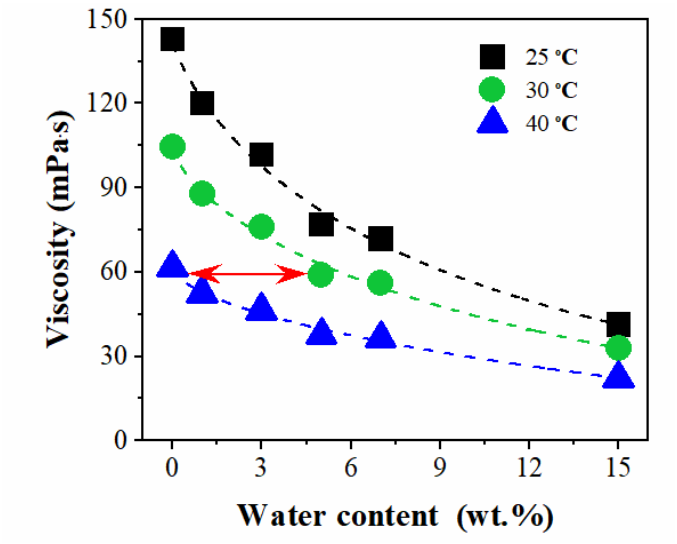

Fig. 3 Viscosity of [EMIM][OAc] and [EMIM][OAc]-water mixtures as a function of water content at various temperatures. The arrows show the same viscosity of [EMIM][OAc] at 40 °C and of [EMIM][OAc]-5 wt.% water at 30 °C

3.3 Kinetics of fiber dissolution and swelling

As mentioned in the Experimental section, in our set-up both fiber ends were fixed as the goal is to quantitatively analyze the kinetics of fiber behavior and thus fiber displacements should be prevented. It has been reported that depending on the solvent power, uniaxial elongational stress applied on a fiber may influence its dissolution (Le Moigne et al. 2010). We tested if fixed fiber ends modified its behavior in the solvents used. Two cases should be distinguished: good cellulose solvents and moderate/bad ones (Cuissinat et al.

2006). [EMIM][OAc] is known to be very good cellulose solvent; in this case fixing the fiber ends only slightly slowed down the dissolution kinetics but did not change the dissolution mechanism (see Supporting Information, Figure S3). In the presence of water, the dissolution capacity of [EMIM][OAc] is known to be decreased (Hauru et al. 2012; Le et al. 2012; Minnick et al. 2016; Olsson et al. 2014); however, fixing fiber ends did not modify its behavior for the given composition of ionic liquid-water (Figure S4). All fibers studied in this work were always analyzed under the same conditions.

3.3.1 Dissolution in [EMIM][OAc]

The examples of fibers' evolution in [EMIM][OAc] at 30 °C are shown in Figure 4 and at other temperatures in Figure S5. All fibers dissolved without swelling, and temperature strongly accelerated the dissolution. While flax, Cordenka and Ioncell-F dissolved radially in a homogeneous way, the dissolution of Ioncell-FL occurred via small fragments exfoliating from fiber surface. This was especially pronounced at higher temperatures (Figure S5d). The reason is that Ioncell-FL contains high amount of hemicellulose and lignin making fiber heterogeneous and allowing solvent penetration in the amorphous domains.

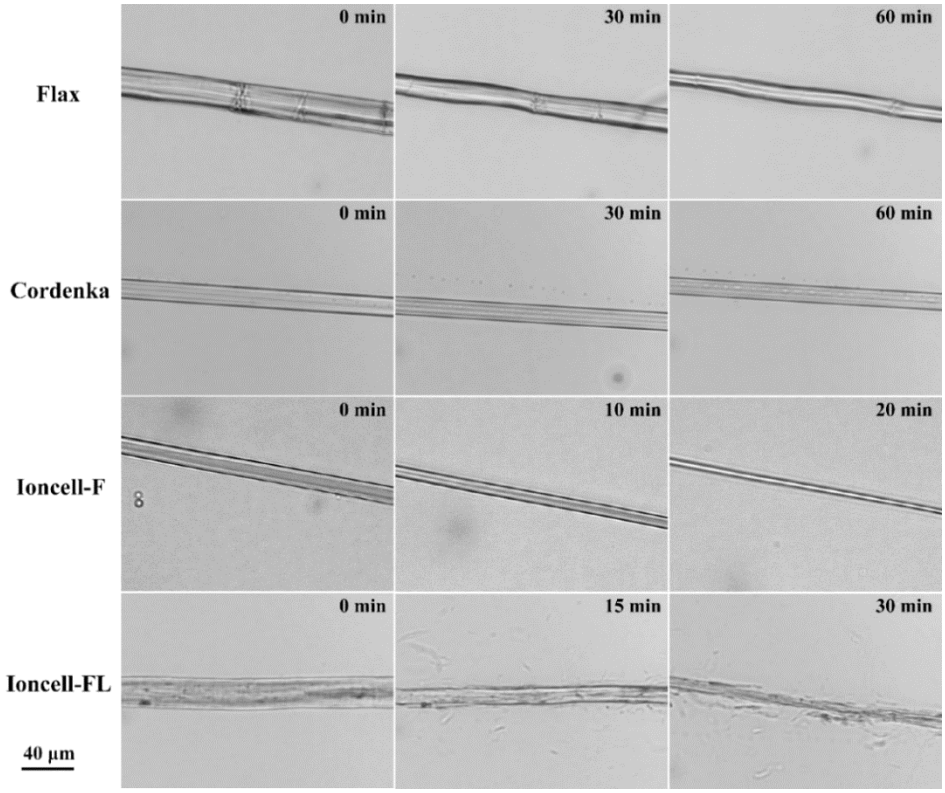

Fig. 4 Optical microscopy images of fibers in [EMIM][OAc] at 30 °C

The normalized diameter D_t/D_0 of each fiber placed in [EMIM][OAc] is plotted in Figure 5 as a function of time at different temperatures. The evolution of the Ioncell-F diameter at 60 °C is not shown as fiber dissolution was too fast. Figure 5 shows the dissolution within the first hour; all fibers were dissolved within 12 hours even at 25 °C. To quantify and compare the dissolution kinetics of different fibers, the dissolution rate R_d was calculated, in the first approximation, as a slope to each set of experimental data approximated by a linear dependence. At all temperatures the dissolution rate follows the order Ioncell-F > Ioncell-FL > flax > Cordenka (Figure 5e) which can be explained by the physico-chemical characteristics of fibers, see Section 3.1 and Table 1. Cordenka has the lowest dissolution rate as it has the lowest accessibility as determined by DVS. The second lowest dissolution rate shows flax, mainly due to its hierarchical morphology together with high molecular weight cellulose. Ioncell-F has a higher dissolution rate as compared to that of Ioncell-FL. We speculate that slower dissolution of Ioncell-FL is due to the presence of lignin (Table 1) which is known to slow down cellulose dissolution (Isogai and Atalla 1998; Shi et al. 2014).

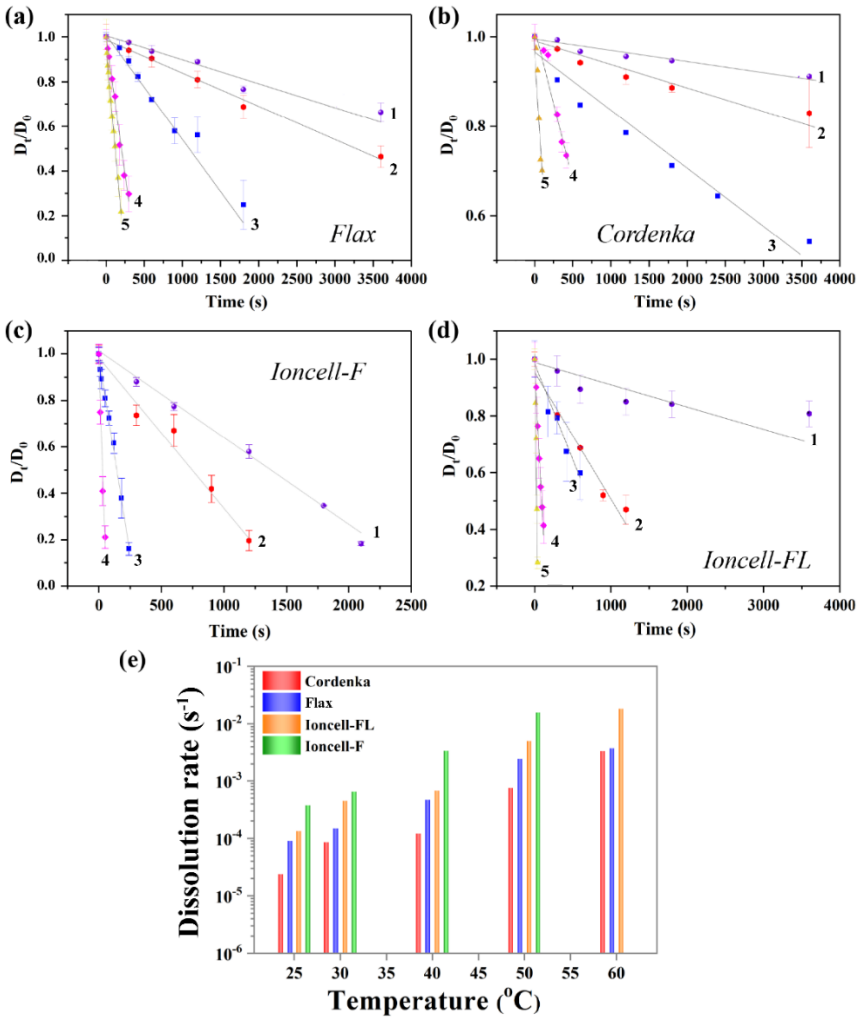

Fig. 5 Evolution of flax (a), Cordenka (b), Ioncell-F (c) and Ioncell-FL (d) normalized diameter as a function of time at 25 ℃ (1), 30 ℃ (2), 40 ℃ (3), 50 ℃ (4) and 60 ℃ (5) in [EMIM][OAc] and the dissolution rate of all fibers as a function of temperature (e)

Figure 5 shows that increasing the temperature increases the dissolution rate, which is expected due to quicker solvent diffusion in a medium of lower viscosity. The dependence of [EMIM][OAc] viscosity η on temperature can be approximated by Arrhenius-type law (Figure S6a) (Gericke et al. 2009):

$$\eta \sim \exp(\frac{E_v}{RT}) \quad (4)$$

where T is temperature in K, R is universal gas constant and E_v the activation energy of viscous flow. The rate of fiber dissolution R_d can also be roughly approximated by the same law, analogous to other processes' rates (Powell et al. 1941). In this case, the viscosity in eq.4 is substituted by R_d and the activation energy of viscous flow by the activation energy of dissolution E_d. Figure S6b shows a linear dependence of $\ln R_d$ on $1/T$. As far as both solvent viscosity and dissolution rate follow Arrhenius-type dependence as a function of inverse temperature, it was logical to probe their direct correlation in natural logarithm form:

$$lnR_d \sim \frac{E_d}{E_v}\, ln\eta \quad (5)$$

Figure 6 shows a linear decrease of $\ln R_d$ with the increase of $\ln \eta$, with the slope being the ratio between the activation energies E_d and E_v. All dependences can be roughly approximated by linear trends confirming the applicability of this analysis for [EMIM][OAc] as solvent of cellulose fibers.

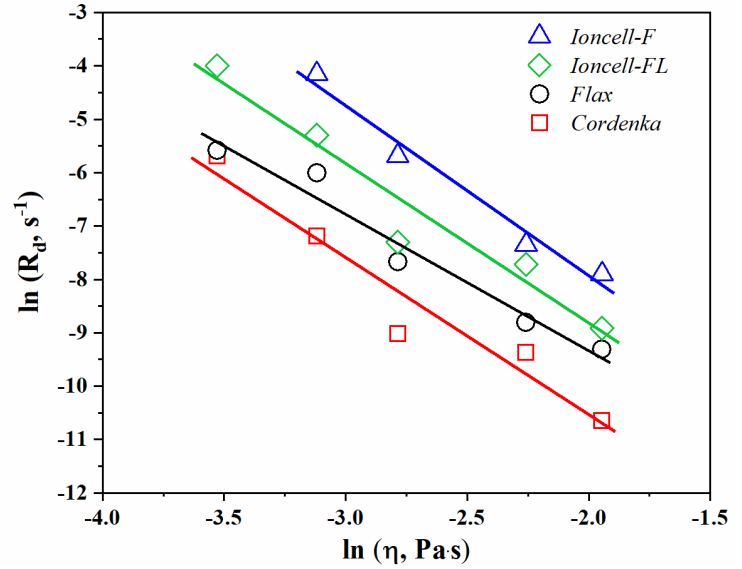

Fig. 6 Dissolution rate as a function of [EMIM][OAc] viscosity

3.3.2 Dissolution and swelling of fibers in [EMIM][OAc]-5 wt.% water

The presence of a low amount of water, 5 wt.%, should decrease the dissolution power but still allow the dissolution (Figure 2). Examples of fiber behavior in [EMIM][OAc]-5 wt.% water at 30 °C is presented in Figure 7. All man-made fibers were dissolving in this solvent in a similar manner as in [EMIM][OAc]. In contrast, flax was only swelling showing a core-shell structure and was not dissolved in [EMIM][OAc]-5 wt.% after 18 hours. This is the direct indication of the decreased solvent power of [EMIM][OAc]-5 wt.% water apparent for a natural fiber. No ballooning was observed irrespective of whether the fiber ends were fixed or free (see Figure S4). This is in accordance with previous observations for flax swelling in NMMO containing more than 19-20% of water (Cuissinat et al. 2008).

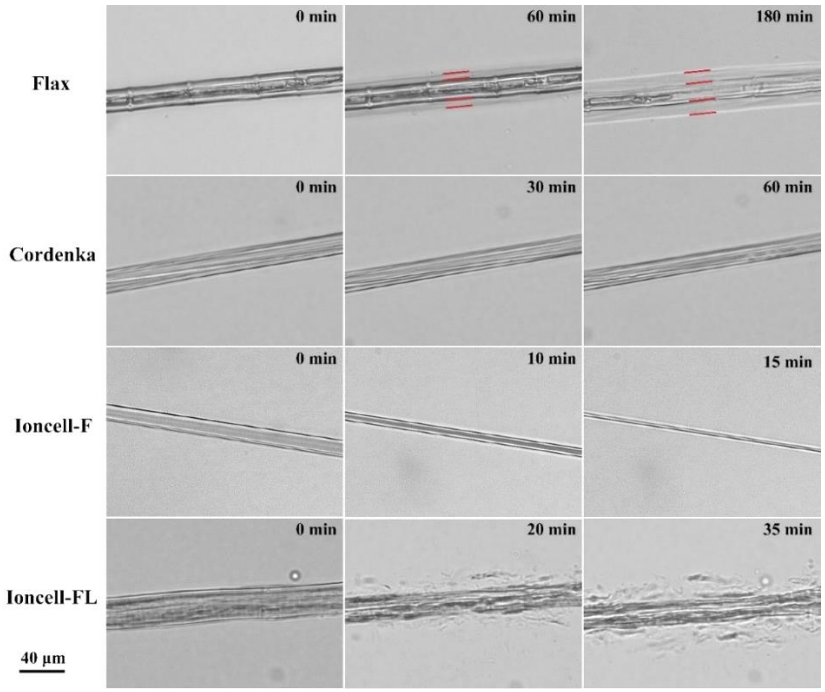

Fig. 7 Optical microscopy images of the fiber evolution in time in [EMIM][OAc]-5% water at 30 ℃. Red marks show core-shell structure

The addition of water to the ionic liquid strongly decreases its viscosity as shown in Figure 3, which could, theoretically, increase the dissolution rate according to Figure 6. It was interesting to check which input, solvent quality or viscosity, is more important in controlling the dissolution rate. To answer this question, the fibers' behavior in two solvent systems with the same viscosity was compared: [EMIM][OAc]-5 wt.% water at 30 °C and neat [EMIM][OAc] at 40 °C, see Figure 3. Figure 8 shows the evolution of the normalized diameter in these two solvents for each fiber. Except for flax which is not dissolving in [EMIM][OAc]-5 wt.% water, the dissolution rate of man-made fibers decreased in the presence of water as compared to the neat ionic liquid. This indicates that the dissolution kinetics of fibers is governed by the solvent power rather than viscosity of the solvent system. The comparison of D_t/D_0 of Cordenka, Ioncell-F and Ioncell-FL as a function of time at 30 °C in [EMIM][OAc]-5 wt.% water is presented in Figure 9; it shows the same dissolution rate order as for neat [EMIM][OAc]: Ioncell-F > Ioncell-FL > Cordenka, see the values in Supporting information Table S1.

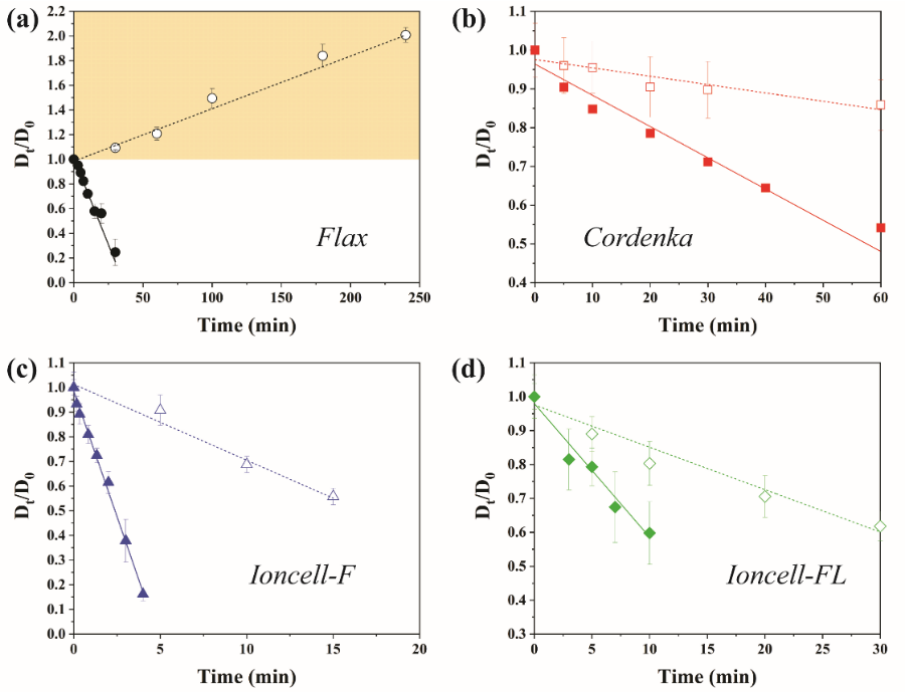

397

398 **Fig. 8** Comparison of the normalized diameter of flax (a), Cordenka (b), Ioncell-F (c) and
399 Ioncell-FL (d) as a function of time in the solvents of the same viscosity: [EMIM][OAc] at
400 40 °C (solid symbol) and [EMIM][OAc]-5 wt.% water at 30 °C (open symbol). Shaded area
401 shows swelling

402

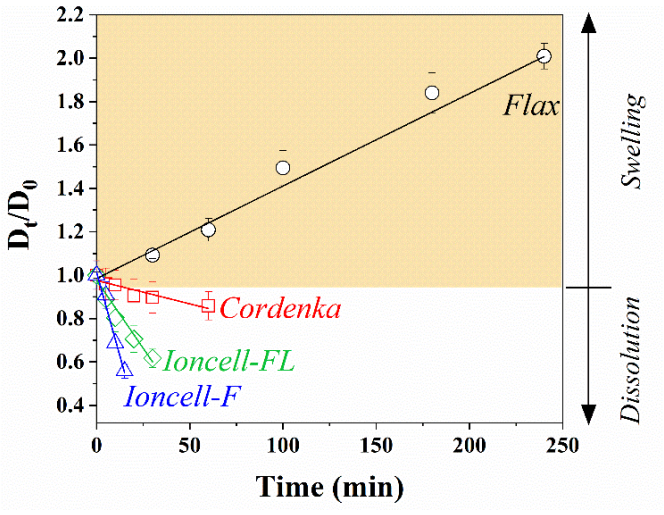

403

404 **Fig. 9** Comparison of the normalized diameter of flax, Cordenka, Ioncell-F and Ioncell-FL
405 as a function of time at 30 °C in [EMIM][OAc]-5 wt.% water mixture solvent

406

3.3.3 Swelling of fibers in [EMIM][OAc]-15 wt.% water

The addition of 15 wt.% of water to [EMIM][OAc] pushes this solvent system to the limit of the solubility region, see Figure 2. Figure 10 provides the representative optical microscope images of all four fibers in [EMIM][OAc]-15 wt.% water at 30 ℃. No fiber dissolved; all were swelling via core-shell structure similar to flax in [EMIM][OAc]-5 wt.% water. Cordenka showed poor swelling in these conditions. To check that it can swell in this solvent a test at 50 °C was performed, and it showed that temperature increase induced higher swelling (Figure S7).

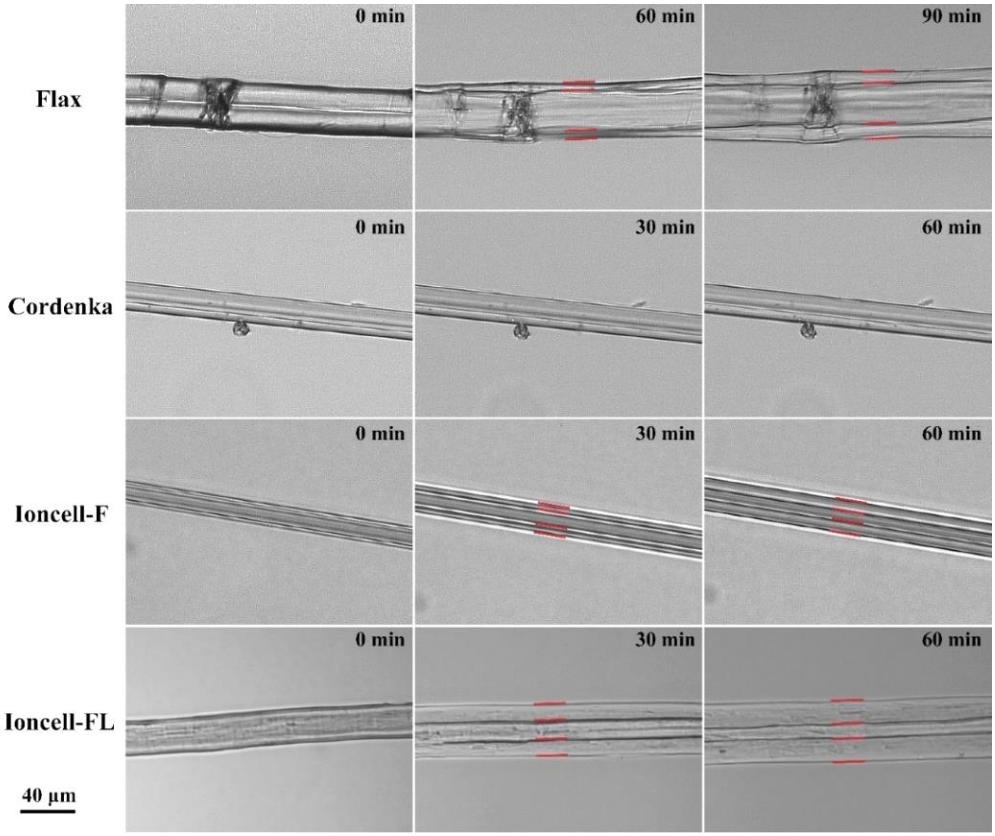

Fig. 10 Optical microscopy images of fibers in [EMIM][OAc]-15% water at 30 ℃. Red marks show core-shell structure

The evolution of the normalized diameter of flax, Cordenka, Ioncell-F and Ioncell-FL in [EMIM][OAc]-15 wt.% water as function of time at 30 ℃ is compared in Figure 11. As well as for fibers' dissolution rate (Figure 5), the swelling rate follows the same order: Ioncell-F > Ioncell-FL > flax > Cordenka.

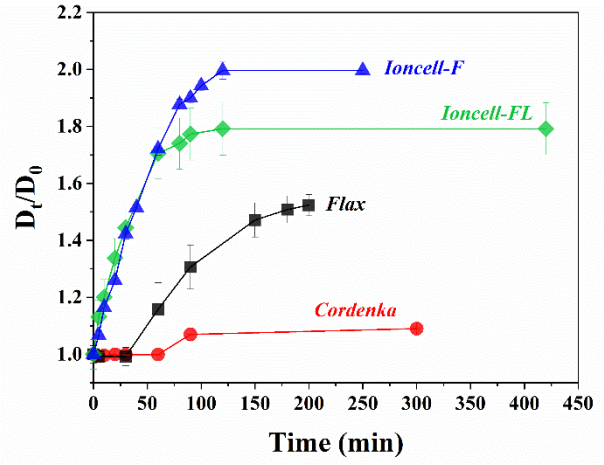

Fig. 11 Comparison of the normalized diameter of flax, Cordenka, Ioncell-F and Ioncell-FL as a function of time at 30 ℃ in [EMIM][OAc]-15 wt.% water solvent

4 Discussion

The comparison of the behavior of all fibers in three solvent systems is summarized in Figure 12. At high solvent power (ionic liquid) and fixed temperature, all fibers dissolve and the dissolution rate is controlled mainly by the fiber accessibility. Within the same family of man-made fibers, Ioncell, the presence of lignin slows down the dissolution rate, and Ioncell-FL dissolves via partial fragmentation. With the decrease of solvent power, the nature of fibers, man-made versus natural, becomes the main factor controlling their behavior. Flax, which has a hierarchical structure with strong secondary layer, turned out to be the most "sensitive" to the presence of water. Despite that [EMIM][OAc]-5 wt.% water was expected to dissolve cellulose, flax was only swelling. All fibers had a similar water content at ambient conditions, with flax has the least, thus ruling out that the "intrinsic" water could be the reason of its insolubility in [EMIM][OAc]-5 wt.% water. It should be reminded here that the dissolution experiments were performed in static conditions, without mixing. Finally, in the presence of 15 wt.% water in ionic liquid, all fibers showed only swelling.

The results also reveal that under the same experimental conditions (solvent power and temperature), not only the kinetics of dissolution but also the kinetics of swelling correlate to the accessibility of fibers: man-made Ioncell-type fibers showed the highest dissolution

and swelling rates, followed by flax and finally Cordenka with the lowest rates. Temperature increase amplifies the phenomena but does not change the general trend.

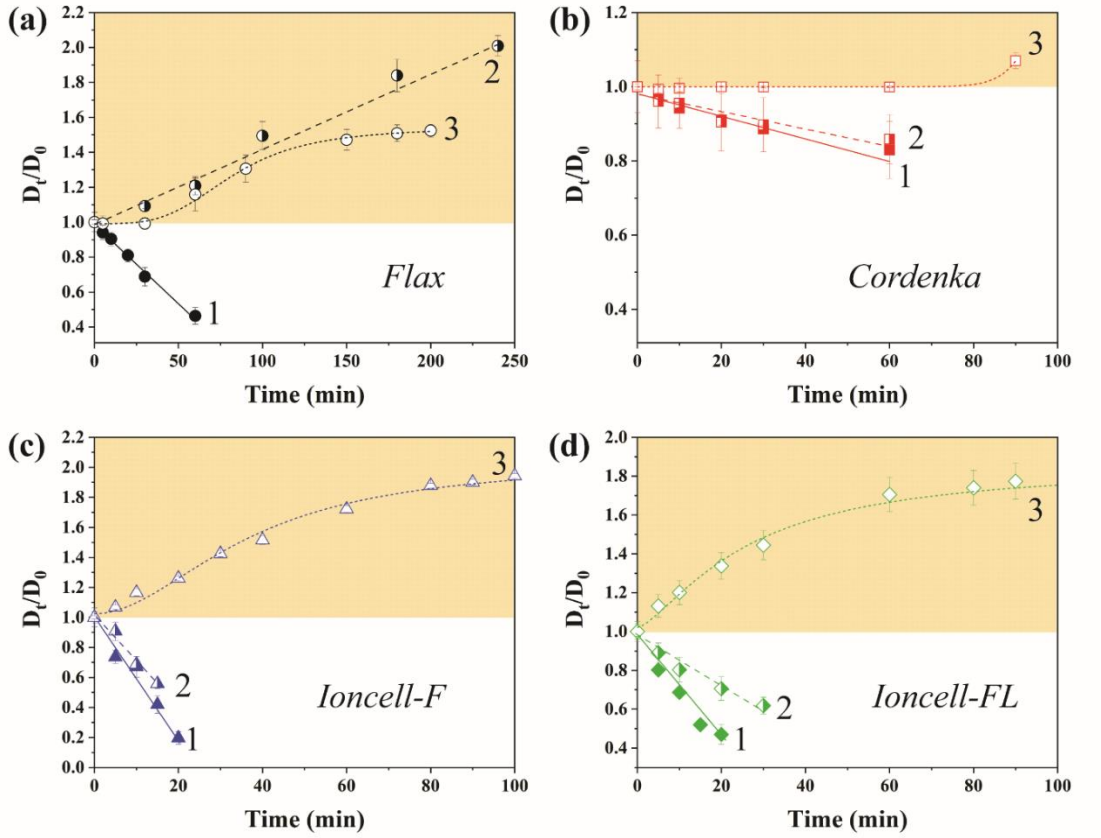

Fig. 12 Comparison of the normalized diameter of flax (a), Cordenka (b), Ioncell-F (c) and Ioncell-FL (d) as a function of time in neat [EMIM][OAc] (1), [EMIM][OAc]-5% water mixture (2) and [EMIM][OAc]-15% water mixture (3) at 30 °C

5 Conclusions

The kinetics of fiber evolution in ionic liquid, [EMIM][OAc], was studied for four cellulose fibers, natural (flax) and man-made: viscose type (Cordenka) and Lyocell-type (Ioncell: one similar to Cordenka in composition (Ioncell-F) and the other one with high amounts of lignin and hemicelluloses (Ioncell-FL)). This set of fibers allowed studying the role of the fiber morphology, accessibility, composition and cellulose molecular weight and crystallinity. Temperature was varied to modify solvent viscosity, and water was added to tune solvent power.

In the case of high solvent power all fibers are radially dissolving. The main factors influencing the dissolution rate are solvent viscosity (for the same type of fiber) and fiber accessibility (for the same solvent temperature), the latter revealed by water vapor sorption. An Arrhenius-type law was applied to both solvent viscosity and dissolution rate resulting in log-log direct correlation between them.

The decrease of solvent quality due to the addition of water showed that despite the decrease in viscosity, the solvent quality controls the kinetics of the fiber behavior. Flax turned out to be the most "sensitive" to the presence of water, since even a moderate amount of water (5 wt.%) in the [EMIM][OAc] leads to fiber homogeneous swelling with a core-shell structure while all man-made fibers were still dissolving under this condition. Further increase of water content induced radial swelling of all fibers but prevented dissolution.

It is remarkable that both the kinetics of dissolution (the cases of all fibers in neat [EMIM][OAc] and all man-made fibers in [EMIM][OAc]-5 wt.% water) and of swelling (the cases of all fibers in [EMIM][OAc]-15 wt.% water) show the same order: Ioncell-F > Ioncell-FL > flax > Cordenka. Rising temperature was found to amplify both the dissolution and swelling phenomena but did not change the observed behavior. The results obtained in this study are important to consider when preparing all-cellulose composites in which complete dissolution is not required and the substrates are typically impregnated under static conditions without mixing.

Acknowledgements: The financial support from Business Finland, Stora Enso Oyj and UPM-Kymmene Oyj is gratefully acknowledged. Authors wish to thank Separation Research Oy Ab and Fibertus Oy for collaboration. We thank Gabriel Monge (CEMEF, MINES ParisTech) and Leena Pitänen (Aalto University) for XRD and GPC measurement, respectively.

References

Abu-Rous M, Varga K, Bechtold T, Schuster KC (2007) A new method to visualize and characterize the pore structure of TENCEL®(Lyocell) and other man-made cellulosic fibres using a fluorescent dye molecular probe. J Appl Polym Sci 106:2083-91.

Andanson JM, Bordes E, Devémy J, Leroux F, Pádua AA, Gomes MF (2014) Understanding the role of co-solvents in the dissolution of cellulose in ionic liquids. Green Chem 16:2528-38.

Asaadi S, Hummel M, Ahvenainen P, Gubitosi M, Olsson U, Sixta H (2018) Structural analysis of Ioncell-F fibres from birch wood. Carbohydr Polym 181:893-901.

Baley C (2000) Analysis of the flax fibres tensile behaviour and analysis of the tensile stiffness increase. Compos Part A-Appl S 33:939-48.

Bolton AJ (1994) Natural fibers for plastic reinforcement. Mater Technol 9:12-20.

Brückner S (2000) Estimation of the background in powder diffraction patterns through a robust smoothing procedure. J Appl Crystallogr 33: 977-979.

Budtova T, Navard P (2016) Cellulose in NaOH–water based solvents: a review. Cellulose 23:5-5.

Budtova T (2019) Cellulose II aerogels: A review. Cellulose 26:81-121.

Charlet K, Jernot JP, Eve S, Gomina M, Bréard J (2010) Multi-scale morphological characterisation of flax: From the stem to the fibrils. Carbohydr Polym 82:54-61.

Chaudemanche C, Navard P (2011) Swelling and dissolution mechanisms of regenerated Lyocell cellulose fibers. Cellulose 18:1-5.

Chen F, Kan Z, Hua S, Liu Z, Yang M (2015) A new understanding concerning the influence of structural changes on the thermal behavior of cellulose. J Polym Res 22:225.

Chen F, Sawada D, Hummel M, Sixta H, Budtova T (2020) Unidirectional all-cellulose composites from flax via controlled impregnation with ionic liquid. Polymers 12:1010.

Cuissinat C, Navard P (2006) Swelling and Dissolution of Cellulose Part 1: Free floating cotton and wood fibres in N-methylmorpholine-N-oxide–water mixtures. Macromol Symp 244:1-18.

Cuissinat C, Navard P (2008) Swelling and dissolution of cellulose, Part III: plant fibres in aqueous systems. Cellulose 15:67-74.

Fink HP, Weigel P, Purz HJ, Ganster J (2001) Structure formation of regenerated cellulose materials from NMMO-solutions. Prog Polym Sci 26:1473-524.

Frost K, Kaminski D, Kirwan G, et al (2009) Crystallinity and structure of starch using wide angle X-ray scattering. Carbohydr Polym 78: 543-548.

Fukaya Y, Sugimoto, A, Ohno, H (2006) Superior Solubility of Polysaccharides in Low Viscosity, Polar, and Halogen-Free 1,3-Dialkylimidazolium Formates. Biomacromolecules 12:3295−3297.

Gericke M, Schlufter K, Liebert T, Heinze T, Budtova T (2009) Rheological properties of cellulose/ionic liquid solutions: from dilute to concentrated states. Biomacromolecules 10:1188-94.

Gross AS, Chu JW (2010) On the molecular origins of biomass recalcitrance: the interaction network and solvation structures of cellulose microfibrils. J Phys Chem B 114:13333-41.

Hall CA, Le KA, Rudaz C, Radhi A, Lovell CS, Damion RA, Budtova T, Ries ME (2012) Macroscopic and microscopic study of 1-ethyl-3-methyl-imidazolium acetate–water mixtures. J Phys Chem B 116:12810-8.

Hauru LK, Hummel M, King AW, Kilpelainen I, Sixta H (2012) Role of solvent parameters in the regeneration of cellulose from ionic liquid solutions. Biomacromolecules 13:2896-905.

Huber T, Müssig J, Curnow O, Pang S, Bickerton S, Staiger MP (2012) A critical review of all-cellulose composites. J Mater Sci 47(3):1171-86.

Isogai A, Atalla RH (1998) Dissolution of cellulose in aqueous NaOH solutions. Cellulose 5:309-19.

Janson J (1970) Calculation of the polysaccharide composition of wood and pulp. Pap Puu-Pap Tim 52:323-9.

Klemm D, Heublein B, Fink HP, Bohn A (2005) Cellulose: fascinating biopolymer and sustainable raw material. Angew Chem Int Ed Engl 44:3358-93.

Korhonen O, Sawada D, Budtova T (2019) All-cellulose composites via short-fiber dispersion approach using NaOH–water solvent. Cellulose. 26:4881-93.

Kreze T, Malej S (2003) Structural characteristics of new and conventional regenerated cellulosic fibers. Text Res J 73:675-84.

Le KA, Sescousse R, Budtova T (2012) Influence of water on cellulose-EMIMAc solution properties: a viscometric study. Cellulose 19:45-54.

Le Moigne N, Montes E, Pannetier C, Höfte H, Navard P (2008) Gradient in dissolution capacity of successively deposited cell wall layers in cotton fibres Macromol Symp 262:65-71.

Le Moigne N, Jardeby K, Navard P (2010) Structural changes and alkaline solubility of wood cellulose fibers after enzymatic peeling treatment. Carbohydr Polym 79:325-32.

Le Moigne N, Spinu M, Heinze T, Navard P (2010) Restricted dissolution and derivatization capacities of cellulose fibres under uniaxial elongational stress. Polymer 51:447-53.

Ma Y, Asaadi S, Johansson LS, Ahvenainen P, Reza M, Alekhina M, Rautkari L, Michud A, Hauru L, Hummel M, Sixta H (2015) High-strength composite fibers from cellulose–lignin blends regenerated from ionic liquid solution. ChemSusChem 8:4030-9.

Ma Y, Stubb J, Kontro I, Nieminen K, Hummel M, Sixta H (2018) Filament spinning of unbleached birch kraft pulps: Effect of pulping intensity on the processability and the fiber properties. Carbohydr Polym 179:145-51.

Mäkelä V, Wahlström R, Holopainen-Mantila U, Kilpeläinen I, King AW (2018) Clustered single cellulosic fiber dissolution kinetics and mechanisms through optical microscopy under limited dissolving conditions. Biomacromolecules 2018 19:1635-45.

McCormick CL, Callais PA, Hutchinson Jr BH (1985) Solution studies of cellulose in lithium chloride and N, N-dimethylacetamide. Macromolecules 18: 2394-2401.

Minnick DL, Flores RA, DeStefano MR, Scurto AM (2016) Cellulose solubility in ionic liquid mixtures: temperature, cosolvent, and antisolvent effects. J Phys Chem B 120:7906-19.

Moryganov AP, Zavadskii AE, Stokozenko VG. (2018) Special features of X-ray analysis of cellulose crystallinity and content in flax fibres. Fibre Chem 49:382-7.

Okubayashi S, Griesser UJ, Bechtold T (2004) A kinetic study of moisture sorption and desorption on lyocell fibers. Carbohydr Polym 58(3):293-9.

Okubayashi S, Griesser UJ, Bechtold T (2005) Water accessibilities of man-made cellulosic fibers–effects of fiber characteristics. Cellulose 12:403-10.

566 Olsson C, Idström A, Nordstierna L, Westman G (2014) Influence of water on swelling and dissolution of
567 cellulose in 1-ethyl-3-methylimidazolium acetate. Carbohydr Polym 99:438-46.
568 Parviainen H, Parviainen A, Virtanen T, Kilpeläinen I, Ahvenainen P, Serimaa R, Grönqvist S, Maloney T,
569 Maunu SL (2014) Dissolution enthalpies of cellulose in ionic liquids. Carbohydr Polym 113:67-76.
570 Peng H, Dai G, Wang S, Xu H (2017) The evolution behavior and dissolution mechanism of cellulose in
571 aqueous solvent. J Mol Liq 241:959-66.
572 Placet V, Trivaudey F, Cisse O, Gucheret-Retel V, Boubakar ML (2012) Diameter dependence of the apparent
573 tensile modulus of hemp fibres: A morphological, structural or ultrastructural effect? Compos Part A-
574 Appl S 43:275-87.
575 Powell RE, Roseveare WE, Eyring H (1941) Diffusion, thermal conductivity, and viscous flow of liquids. Ind
576 Eng Chem 33:430-5.
577 Ragauskas AJ, Williams CK, Davison BH, Britovsek G, Cairney J, Eckert CA, Frederick WJ, Hallett JP, Leak
578 DJ, Liotta CL, Mielenz JR (2006) The path forward for biofuels and biomaterials. Science 311:484-
579 9.
580 Rong MZ, Zhang MQ, Liu Y, Yang GC, Zeng HM (2001) The effect of fiber treatment on the mechanical
581 properties of unidirectional sisal-reinforced epoxy composites. Compos Sci Technol 61:1437-47.
582 Rous MA, Ingolic E, Schuster KC (2006) Visualisation of the fibrillar and pore morphology of cellulosic fibres
583 applying transmission electron microscopy. Cellulose 13:411-9.
584 Rous MA, Varga K, Bechtold T, Schuster KC (2007) A new method to visualize and characterize the pore
585 structure of TENCEL®(Lyocell) and other man-made cellulosic fibres using a fluorescent dye
586 molecular probe. J Appl Polym Sci 106:2083-91.
587 Savitzky A, Golay MJ (1964) Smoothing and differentiation of data by simplified least squares procedures.
588 Anal Chem 36:1627-1639.
589 Shi Z, Yang Q, Cai J, Kuga S, Matsumoto Y (2014) Effects of lignin and hemicellulose contents on dissolution
590 of wood pulp in aqueous NaOH/urea solution. Cellulose 21:1205-15.
591 Siroka B, Noisternig M, Griesser UJ, Bechtold T (2008) Characterization of cellulosic fibers and fabrics by
592 sorption/desorption. Carbohydr Res 343:2194-9.
593 Sixta H, Michud A, Hauru L, et al (2015) Ioncell-F: a high-strength regenerated cellulose fibre. Nord Pulp
594 Paper Res J, 30:43-57.
595 Soykeabkaew N, Nishino T, Peijs T (2009) All-cellulose composites of regenerated cellulose fibres by surface
596 selective dissolution. Compos Part A-Appl S 40:321-8.
597 Spange S, Reuter A, Vilsmeier E, Heinze T, Keutel D, Linert WJ (1998) Determination of empirical polarity
598 parameters of the cellulose solvent N, N-dimethylacetamide/LiCl by means of the solvatochromic
599 technique. Polym Sci Part A: Polym Chem 36: 1945−1955.
600 Swatloski R P, Spear S K, Holbrey J D, et al (2002) Dissolution of cellulose with ionic liquids. J Am Chem
601 Soc 124: 4974-4975.
602 Takashi N, Ikuyo M, Koichi H (2004) All-cellulose composite. Macromolecules 37:7683-7.
603 Xie Y, Hill CA, Jalaludin Z, Curling SF, Anandjiwala RD, Norton AJ, Newman G (2011) The dynamic water
604 vapour sorption behaviour of natural fibres and kinetic analysis using the parallel exponential kinetics
605 model. J Mater Sci 46(2):479-89.

606 Yan L, Chouw N, Jayaraman K (2014) Flax fibre and its composites–A review. Compos Part B-Eng 56:296-
607 317.
608
609

610 **Figure legends**

611

612 **Fig. 1** Cellulose molecular mass distribution (a) and X-ray diffraction profiles (b) of flax,
613 Cordenka, Ioncell-F and Ioncell-FL

614 **Fig. 2** β (red symbols) and β−α (blue symbols) plotted against water content in IL
615 [EMIM][OAc] at 25 ℃ (solid symbol) and 60 ℃ (open symbol)

616 **Fig. 3** Viscosity of [EMIM][OAc] and [EMIM][OAc]-water mixtures as a function of water
617 content at various temperatures. The arrows show the same viscosity of [EMIM][OAc] at 40
618 °C and of [EMIM][OAc]-5 wt.% water at 30 °C

619 **Fig. 4** Optical microscopy images of fibers in [EMIM][OAc] at 30 ℃

620 **Fig. 5** Evolution of flax (a), Cordenka (b), Ioncell-F (c) and Ioncell-FL (d) normalized
621 diameter as a function of time at 25 ℃ (1), 30 ℃ (2), 40 ℃ (3), 50 ℃ (4) and 60 ℃ (5) in
622 [EMIM][OAc] and the dissolution rate of all fibers as a function of temperature (e)

623 **Fig. 6** Dissolution rate as a function of [EMIM][OAc] viscosity

624 **Fig. 7** Optical microscopy images of the fiber evolution in time in [EMIM][OAc]-5% water
625 at 30 ℃. Red marks show core-shell structure

626 **Fig. 8** Comparison of the normalized diameter of flax (a), Cordenka (b), Ioncell-F (c) and
627 Ioncell-FL (d) as a function of time in the solvents of the same viscosity: [EMIM][OAc] at
628 40 °C (solid symbol) and [EMIM][OAc]-5 wt.% water at 30 ℃ (open symbol). Shaded area
629 shows swelling

630 **Fig. 9** Comparison of the normalized diameter of flax, Cordenka, Ioncell-F and Ioncell-FL
631 as a function of time at 30 ℃ in [EMIM][OAc]-5 wt.% water mixture solvent

632 **Fig. 10** Optical microscopy images of fibers in [EMIM][OAc]-15% water at 30 ℃. Red
633 marks show core-shell structure

634 **Fig. 11** Comparison of the normalized diameter of flax, Cordenka, Ioncell-F and Ioncell-FL
635 as a function of time at 30 ℃ in [EMIM][OAc]-15 wt.% water solvent

636 **Fig. 12** Comparison of the normalized diameter of flax (a), Cordenka (b), Ioncell-F (c) and
637 Ioncell-FL (d) as a function of time in neat [EMIM][OAc] (1), [EMIM][OAc]-5% water
638 mixture (2) and [EMIM][OAc]-15% water mixture (3) at 30 ℃

639

640

641 TOC image

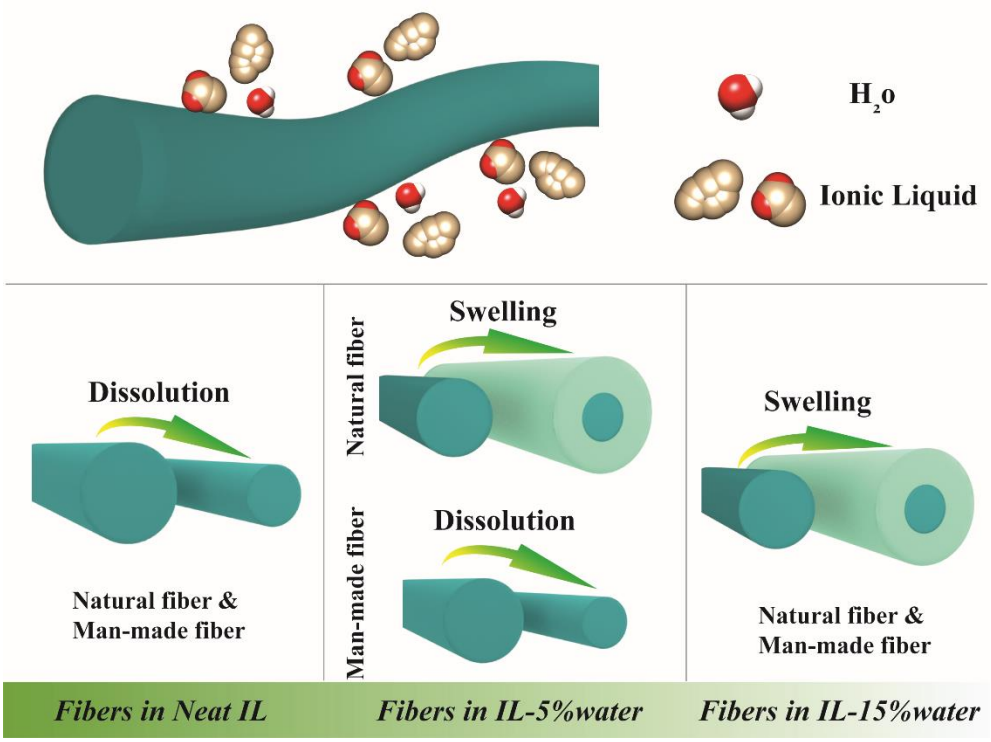

642

643

Supporting Information

Swelling and Dissolution kinetics of Natural and Man-Made Cellulose Fibers in Solvent Power Tuned Ionic Liquid

Feng Chen [a], Daisuke Sawada [a], Michael Hummel [a], Herbert Sixta [a], Tatiana Budtova [a, b, *]

[a] *Department of Bioproducts and Biosystems, School of Chemical Engineering, Aalto University, P.O. Box 16300, 00076 Aalto, Helsinki, Finland;*

[b] *MINES ParisTech, PSL Research University, Center for Materials Forming-CEMEF, UMR CNRS 7635, CS 10207, 06904 Sophia Antipolis, France.*

* Correspondence: tatiana.budtova@mines-paristech.fr, tatiana.budtova@aalto.fi

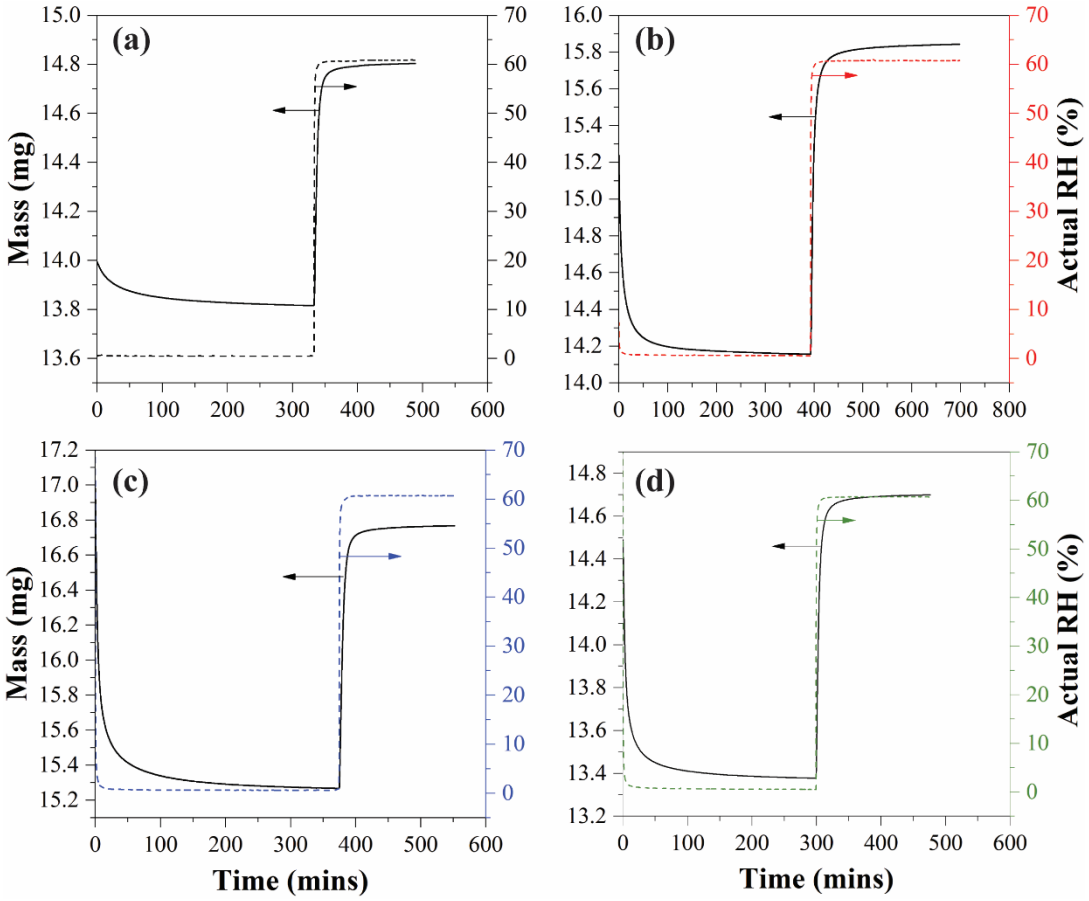

Figure S1.

Equilibrium moisture sorption isotherms of four fibers at 60% RH: (a) flax, (b) Cordenka, (c) Ioncell-FL and (d) Ioncell-F.

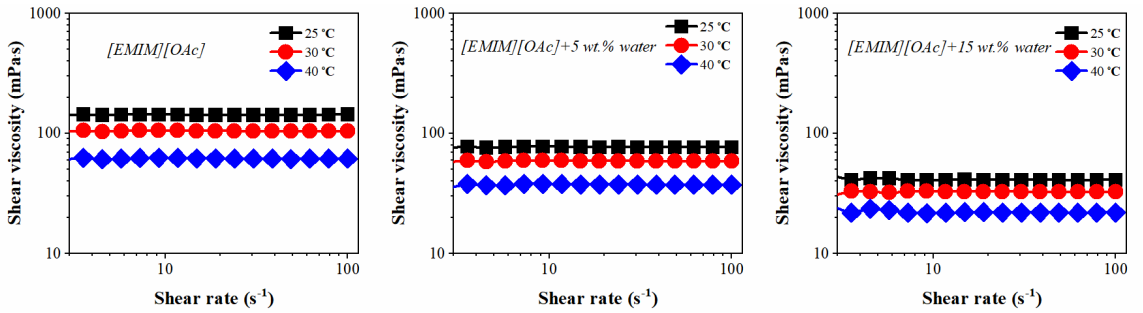

Figure S2.

Shear viscosity of [EMIM][OAc]-water mixture of different water content at 25°C, 30°C and 40°C.

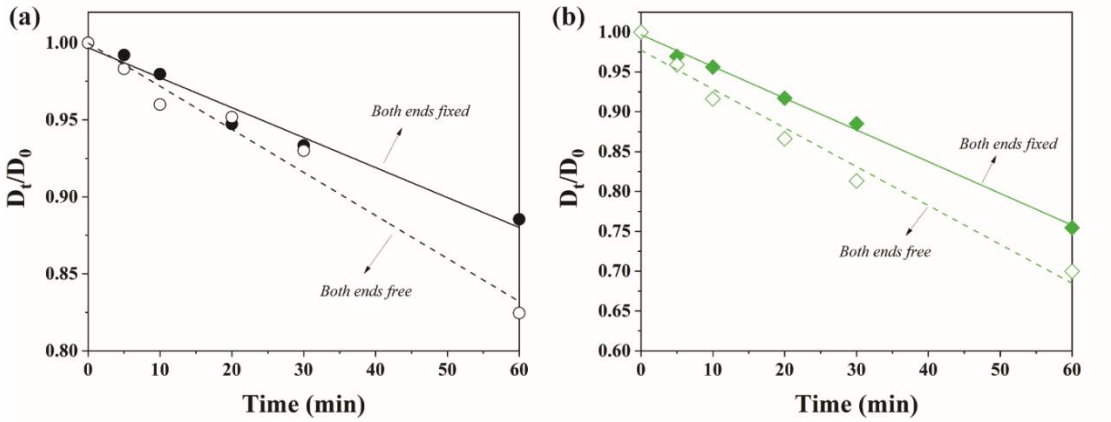

Figure S3.

Comparison of the normalized diameter of natural fiber flax (a) and Ioncell-FL (b) as an example for man-made fiber in IL [EMIM][OAc] with both ends fixed (filled symbol) and free (open symbol).

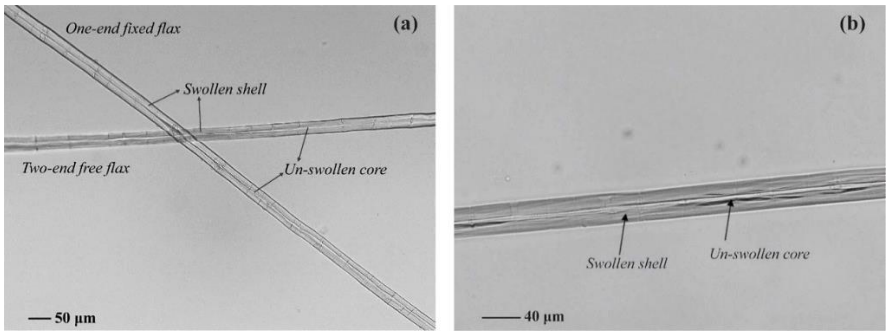

Figure S4.

Optical microscopy images of flax fibers in [EMIM][OAc]-5 wt.% water at 50 ℃: (a) with one end fixed and with both ends free and (b) both ends fixed.

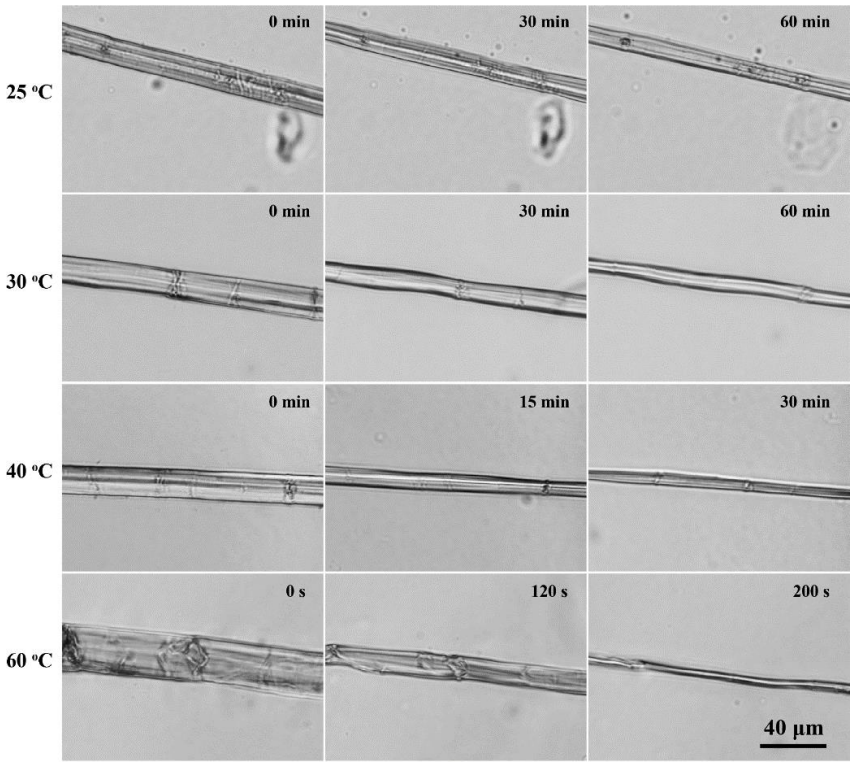

Figure S5a.

Optical microscopy images of flax in [EMIM][OAc] at different temperatures.

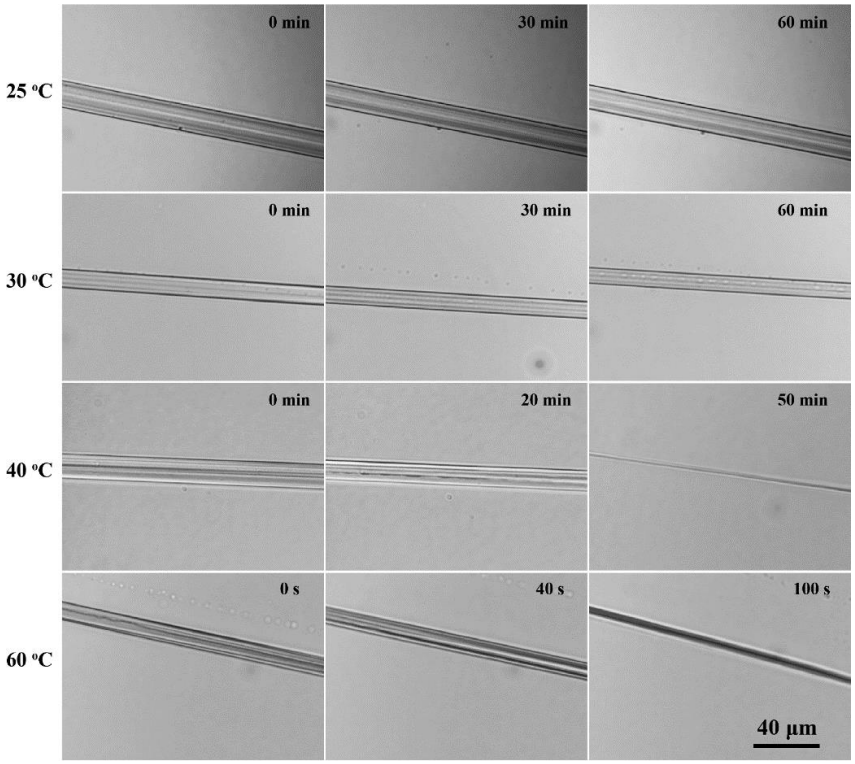

Figure S5b.

Optical microscopy images of Cordenka in [EMIM][OAc] at different temperatures.

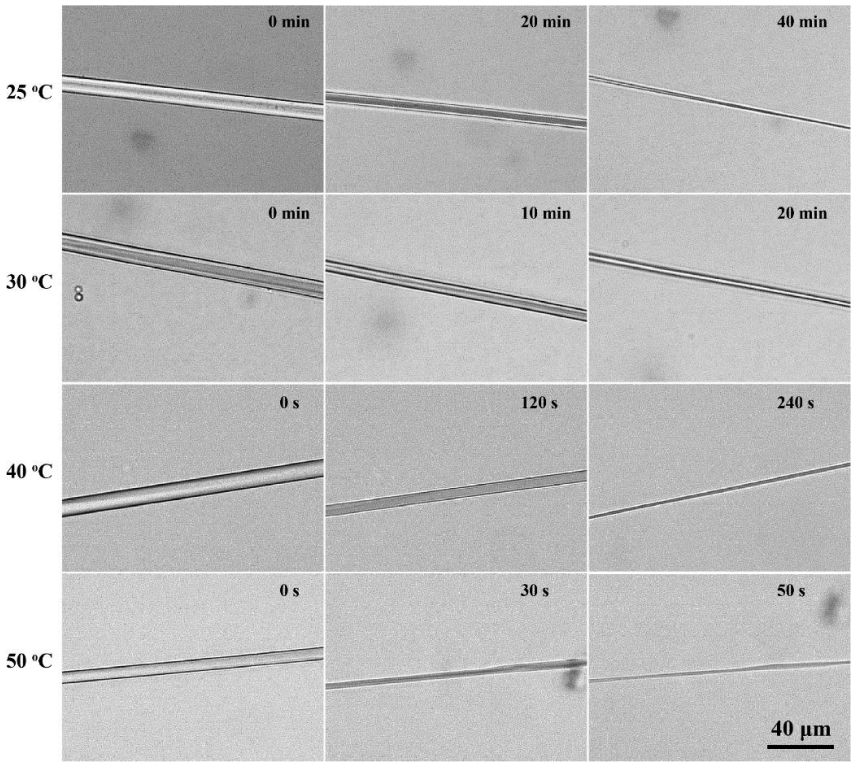

Figure S5c.

Optical microscopy images of Ioncell-F in [EMIM][OAc] at different temperature.

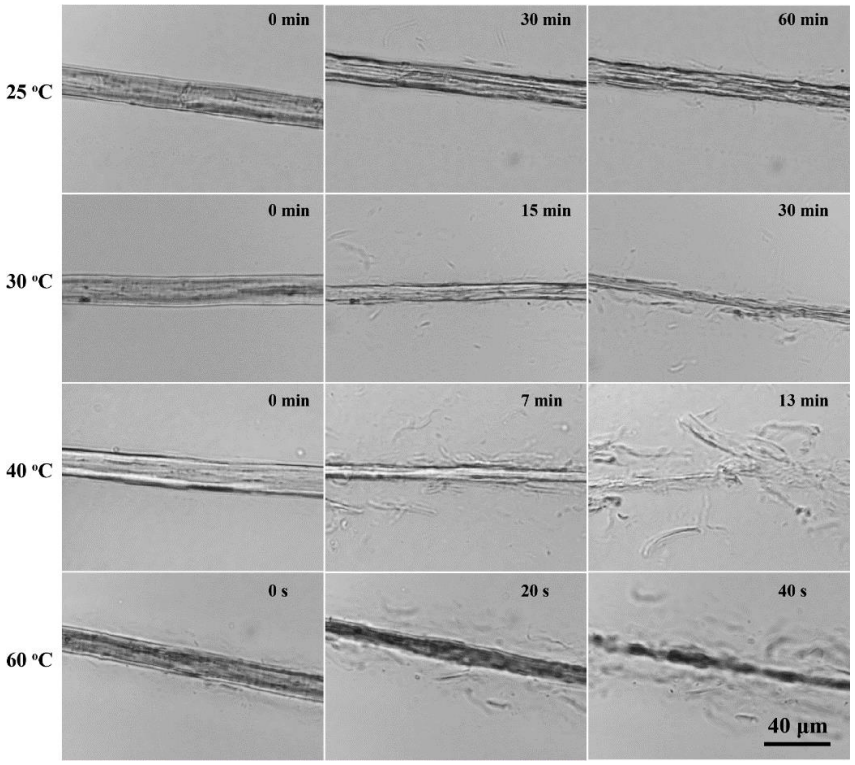

Figure S5d.

Optical microscopy images of Ioncell-FL in [EMIM][OAc] at different temperature.

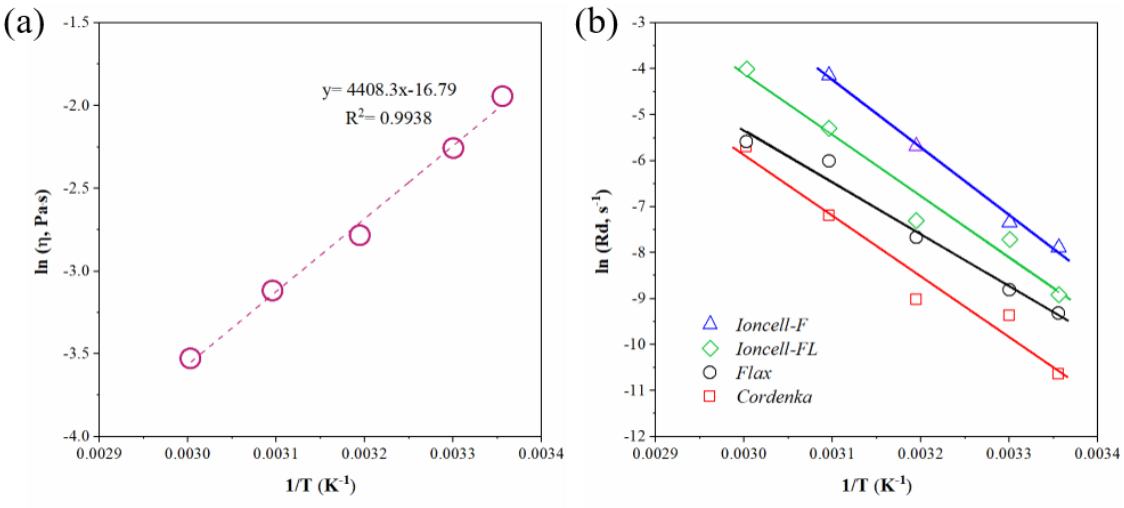

Figure S6.

Arrhenius-type plot for [EMIM][OAc] viscosity (a) and fibers' dissolution rate (b) as a function of inverse temperature.

Table S1. Comparison of dissolution rate of four fibers in [EMIM][OAc] and in [EMIM][OAc]-5 wt.% water at 30°C.

Dissolution rate (s^{-1})	**Cordenka**	**Flax**	**Ioncell-FL**	**Ioncell-F**
in [EMIM][OAc]	$8.51*10^{-5}$	$1.49*10^{-4}$	$4.4*10^{-4}$	$6.48*10^{-4}$
in [EMIM][OAc]-5 wt. % water	$3.58*10^{-5}$	*Swelling*	$2.1*10^{-4}$	$5.1*10^{-4}$

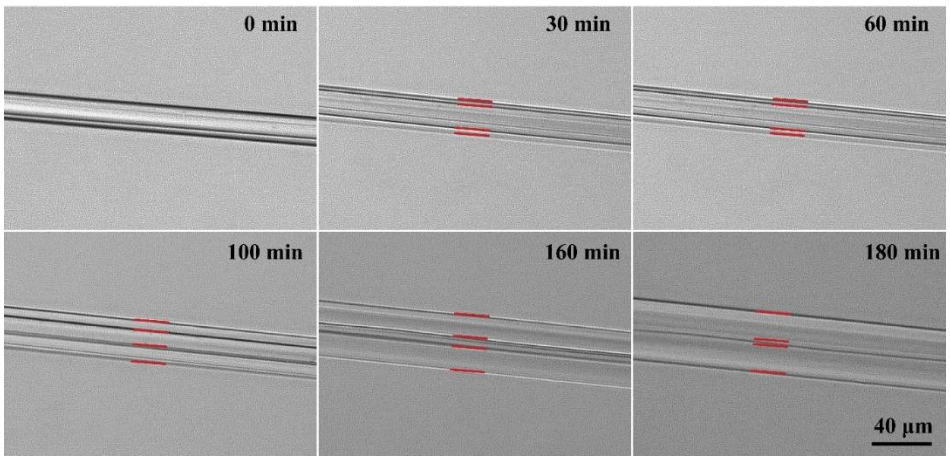

Figure S7.

Optical microscopy images of Cordenka swelling in [EMIM][OAc]+15% water at 50°C.

736